Study on Gravity Changes Induced by Atmospheric Loading(Dissertation_全文)

AUTHOR(S):

Doi, Koichiro

(2)

学位申請論文

STUDY ON GRAVITY CHANGES INDUCED BY ATMOSPHERIC LOADING

(気圧変化により生じた重力変化についての研究)

学位申請者

土井浩一郎

測地学会誌，第 37 巻，第 1 号
(1991)，1-12 頁

Journal of the Geodetic Society of Japan
Vol. 37, No. 1, (1991), pp. 1-12

An Effect of Atmospheric Pressure Changes on the Time Change of Gravity Observed by a Superconducting Gravity Meter

Koichiro DOI, Toshihiro HIGASHI and Ichiro NAKAGAWA

Department of Geophysics, Faculty of Science, Kyoto University

(Received November 13, 1990, Accepted January 22, 1991)

超伝導重力計により観測された重力の時間変化に対する気圧変化の影響

京都大学理学部地球物理学教室　土井浩一郎・東　敏博・中川一郎

(1990 年 11 月 13 日受付，1991 年 1 月 22 日受理)

要　旨

京都大学理学部において，超伝導重力計による重力の時間的変化の連続観測が行なわれている．それによって得られた記録から重力の潮汐変化，線形ドリフトおよび大気による引力が取り除かれ，残った成分が，京都を中心とする角距離 20° までの範囲の気圧分布と荷重グリーン関数を用いて計算された重力に対する弾性変形の効果と比較された．その両者は，いくつかの短期間のくい違いを除き，かなりよく一致している．

気圧荷重に対する弾性変形による効果の大きさが，地球の海洋部分が陸地と同じような応答をする場合，および，海洋部分の応答がゼロの場合の両極端な場合について理論的に求められたが，観測から求められた大きさは両者のほぼ中間の値であった．このような効果が得られた原因として，海洋部分のゼロでない応答，観測点付近の地下構造が平均的な地球のモデルのそれからずれていること，地下水位変動の影響，および，大気の引力計算や荷重変形による効果の計算において行なわれた積分の打ち切り誤差などが考えられる．

ABSTRACT

After eliminating the gravimetric tides, linear drift and atmospheric mass attractions from data which were obtained by a superconducting gravity meter installed at Kyoto, Japan, residuals obtained were compared with estimated elastic effects using the atmospheric pressure distribution within an angular distance of 20° and a load Green's function. The residuals were in considerably good agreement with the estimated elastic effects except for some discrepancies of short periods.

The observed elastic effects took about a middle value between elastic effects estimated for two extreme cases of the earth whose ocean bottom responded perfectly to the atmospheric pressure and of the earth whose ocean bottom did not respond to the atmospheric pressure at all. This result may indicate the presence of non-zero response of the ocean to the atmospheric pressure, the deviation of structure beneath the observation station from the mean earth's structural model, the influence of change in underground water levels, the truncated errors of integration and so on.

1. Introduction

On the continuous observations of gravity change with time by employing a superconducting gravity meter, it was sufficiently improved on its instrumental drift rate and an accuracy of observations as compared with a gravimeter of spring type. For example, an accuracy in continuous observations was about 0.1 μgal for a superconducting gravity meter installed at Kyoto, whereas that for a LaCoste & Romberg gravimeter was about 0.5 μgal. On the other hand, an instrumental drift of the superconducting gravity meter amounted to about 10~15 μgals per month at Kyoto, which corresponded to about one hundredth of that of the LaCoste & Romberg gravimeter.

Before the employment of superconducting gravity meters in continuous observations of gravity change, it was hard to precisely determine a coefficient for the effect of atmospheric pressure changes upon gravity changes because of a large amount of irregular drifts as well as an imperfect buoyancy compensation in the gravimeters of spring type [NAKAGAWA (1962), NAKAI (1975)].

As a result of the very high accuracy of observations, much smaller amount of drift but almost linear drift has been achieved in continuous observations of gravity change executed with the superconducting gravity meter. It is hopeful, nowadays, to find out non-tidal gravity changes accompanied with atmospheric pressure changes through data processing. It is, therefore, important to estimate the atmospheric pressure effects upon gravity changes for the purposes of not only more precise tidal analysis but also the precise investigation of related phenomena. Some methods for the estimation and elimination of atmospheric pressure effects were discussed so far by many researchers [WARBURTON & GOODKIND (1977), SPRATT (1982), OOE & HANADA (1982), RABBEL & ZSCHAU (1985) and VAN DAM & WAHR (1987)].

In the most of those papers, the main subject was how to remove an effect of atmospheric pressures as regarding them as a noise. From a different point of view, a clear appearance of atmospheric pressure effects on gravity records implies that gravity changes enable us to provide some informations of the earth's internal constitution. Since the atmospheric pressure changes, which are caused by the passage of low and high pressures, are regional phenomena on the earth whose scale length is less than a few thousand kilometers, it is considered that the responses induced by loads of such a scale reflect mainly the structure of relatively shallow portion around the observation station. It may therefore be one of methods to investigate an elastic behaviour on the shallow structure of the earth through an observation of gravity changes induced by atmospheric pressure changes.

There are two advantages to use atmospheric pressure changes as an input signal to the earth's system comparing to oceanic tides. One is what the global distribution of atmospheric pressure is well known with short time intervals at least twelve hours. The other is that it is easy to distinguish atmospheric pressure changes from gravimetric tides, because the main frequency range of the changes is about 0.01 cycle/hour, which is corresponding to a few days in periods.

In the present paper, we will devote our interest on non-tidal gravity changes accompanied with atmospheric pressure changes.

2. Observations

Two superconducting gravity meters (S.C.G.) (Model TT-70), N008 and N009, manufactured by GWR Instruments were installed at Kyoto University, Kyoto, Japan (latitude: 35°01′ .66N, longitude: 135°47′ .15E, height: 57.65 m) on March 1988. As the S.C.G. N009 was in disorder after its installation, a continuous observation of gravity changes has commenced with only one superconducting gravity meter (S.C.G. N008). The S.C.G. N009 was reinstalled and adjusted on August 1988. Since then, simultaneous observations of gravity changes with two superconducting gravity meters had been continued to October 1989, when the S.C.G. N008 was sent back to the manufacturer for some experimental repairs about a gravity sensor of the meter.

Digital recording has been performed with two 14-bits digital recorders since January 1989, and all data were registered on 5-inches floppy disk. The output from the gravity meters was filtered and provided to two recording systems; namely, one was high frequency signals ('MODE') and the other was low frequency signals ('TIDE'). The MODE

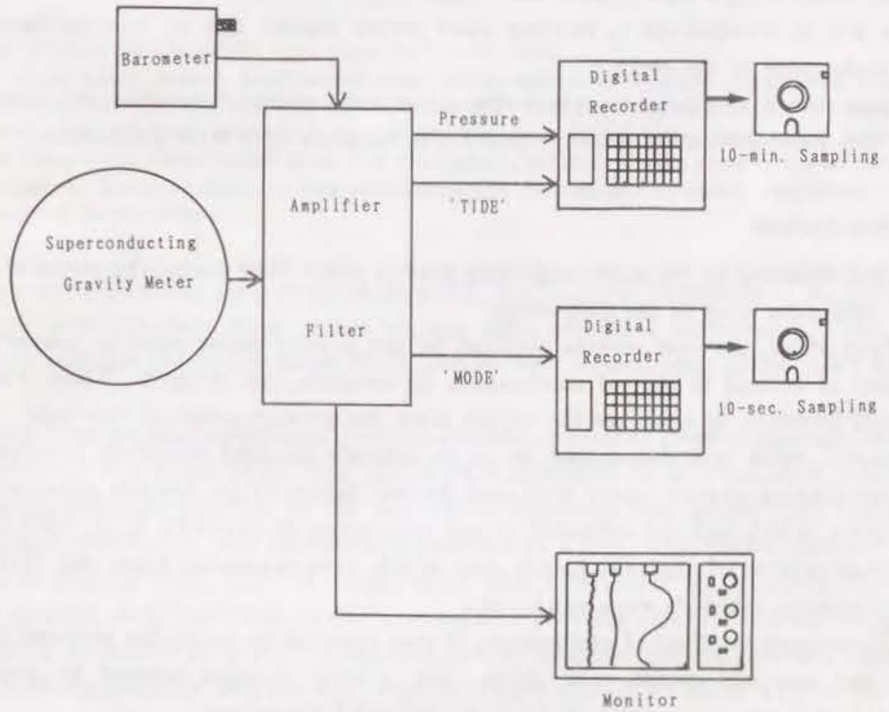

Fig. 1 Data acquisition system.

was sampled at every ten seconds, whereas the TIDE was sampled at every ten minutes. The output of an absolute barometer was also sampled at every ten minutes. The recording system of the gravity meter is illustrated in Fig. 1. A dynamic range of the recording at low frequencies is about 800 μgals ($1\ \mu\text{gal}=1\times10^{-8}$ m/sec) and its resolution is about 0.05 μgal in the unit of acceleration. As for the high frequency signals, a dynamic range is about 20 μgals and a resolution is about 0.002 μgal.

Every ten-minutes and ten-seconds data were acquired by the use of the triggering function of a digital recorder. The digital recorder kept a triggering time, and a clock included in it kept the time with an accuracy better than twenty seconds per month. Because the time of the recorder was adjusted once for ten to fourteen days, and the time accuracy of data was always kept within several seconds.

The superconducting gravity meters were installed in the basement of the building of Department of Geophysics, Kyoto University, and temperature in the observation room was controlled by an air-conditioner within about 0.5°C. Roorn temperature changes affected on electric circuits of analog filter, amplifier, analog-digital converter and so on. But, it was hard to estimate an amount of effect of temperature changes to gravity data. The operation of the air-conditioner caused short period noises with about a few tens of minutes which were due to uneven temperature distribution in the observation room. Such noises were considerably small by covering the front of a dewar of the gravity meter using a right-angled board, but they were not perfectly eliminated. These noises will be troublesome in treating short period signals like as free oscillations and core undertones of the earth.

More detail specifications about the noises and results of simultaneous observations with two superconducting gravity meters will be given in a later publication.

3. Data Analysis

Data obtained by the superconducting gravity meter N009 during the period of January 1-31, 1990 were used in the followings.

First of all, the unit of data obtained by the gravity meter must be converted from the unit of voltage to that of acceleration, for example, unit in μgals. There is no simple method, however, to calibrate the output from the gravity meter of this type. Then, a calibration value was determined so as to coincide the tidal amplitude obtained by the superconducting gravity meter with that derived before by an Askania gravimeter Gs-15 at Kyoto, which had not subjected to any corrections [NAKAGAWA et al. (1975)]. In the following process of analysis, hourly data which were resampled from the 'TIDE' data of ten-minutes intervals were employed.

To estimate an effect of atmosphere, it was required to divide the obtained data into tidal and non-tidal components. After that, gravity changes induced by atmospheric pressure changes were extracted from the non-tidal component.

For eliminating the tidal components which have shorter periods than diurnal tides,

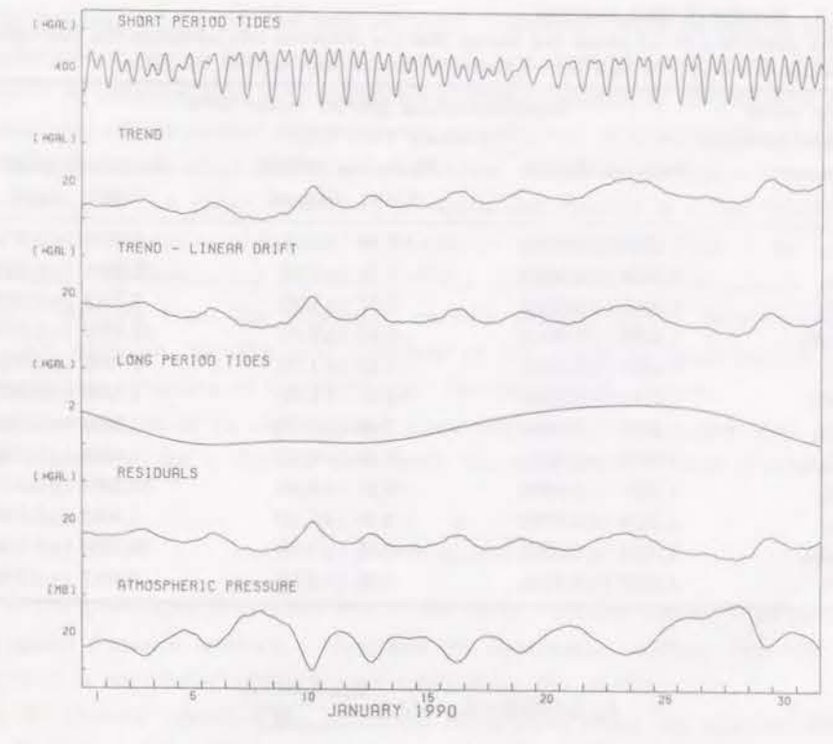

Fig. 2 Data for the period from January 1 to 31, 1990.
From top to bottom, short period tides which consist of diurnal, semidiurnal and terdiurnal tides, trend, obtained by the removal of a linear component, estimated long period tides, residuals obtained by the removal of short period tides, long period tides and linear trend from original data, and atmospheric pressure at the observation station are shown. Scales of short and long period tides are reduced and extended, respectively, compared to the others.

it was applied a Bayesian tidal analysis program 'BAYTAP-G' [ISHIGURO et al. (1984)] by which the observed data were separated into tidal and trend components. The trend component contains the instrumental drift, atmospheric effects, long period tides and so on.

Figure 2 shows tidal component, trend component, corrected trend component obtained by the removal of a linear drift, long period tides estimated by a synthesized method of constituents, residuals obtained by the removal of estimated long period tides from corrected trend component, and atmospheric pressure at Kyoto, which were obtained from the data of January 1-31, 1990. A linear drift was determined by applying the least squares method with the coefficient of atmospheric pressure effects. During the period concerned, a coefficient of gravity changes to atmospheric pressure changes was estimated to be $-0.309\ \mu$gal/millibar and the drift rate was $0.013\ \mu$gal/hour. Since δ-factor for long period tides had not been derived from gravimetric tidal observations at Kyoto, it was estimated by using the following expression,

Table I. Results of tidal analysis

The positive sign of phase lag shows that the observed tide advances the theoretical one, while the negative sign shows that the former lags behind the latter.

Gravity meter : Superconducting gravity meter N009			
Period of analysis : January 1-31, 1990			
Constituent	δ-factor (RMSE)	Phase lag (RMSE) (Unit: degree)	Amplitude (RMSE) (Unit: μgal)
Q_1	1.2096 (±0.0131)	0.46 (±0.62)	6.7616 (±0.0734)
O_1	1.2068 (±0.0020)	0.11 (±0.10)	35.2326 (±0.0598)
M_1	1.2087 (±0.0285)	0.57 (±1.35)	2.7748 (±0.0655)
$P_1S_1K_1$	1.1870 (±0.0011)	−0.80 (±0.05)	48.7370 (±0.0456)
J_1	1.2168 (±0.0224)	−1.03 (±1.05)	2.7936 (±0.0514)
OO_1	1.2131 (±0.0263)	−1.27 (±1.24)	1.5259 (±0.0331)
$2N_2$	1.1761 (±0.0190)	3.00 (±0.92)	1.5003 (±0.0242)
N_2	1.1878 (±0.0021)	−0.59 (±0.10)	11.4488 (±0.0202)
M_2	1.1983 (±0.0003)	−0.21 (±0.02)	60.3265 (±0.0174)
L_2	1.3128 (±0.0258)	−4.38 (±1.12)	1.8682 (±0.0368)
S_2K_2	1.2034 (±0.0007)	−0.66 (±0.03)	28.1839 (±0.0166)
M_3	1.0887 (±0.0102)	0.66 (±0.53)	0.8817 (±0.0082)

$$\delta_{obs}(\mathrm{LONG})=\delta_{obs}(M_2)\times\frac{\delta_{theo}(\mathrm{LONG})}{\delta_{theo}(M_2)}$$
$$=1.1983\times\frac{1.1575}{1.1560}$$

where δ_{obs} and δ_{theo} mean observed and theoretical δ-factors, respectively. The sum of amplitudes of theoretical long period tides which were multiplied by the above-given δ-factor was about 1 μgal for this period.

Results of tidal analysis for short period tides are listed in Table I, which was obtained from one-month's data of January 1-31, 1990. No correction for oceanic tides was made.

4. Estimation of atmospheric pressure effects

After the removal of the linear drift and theoretically estimated long period tides from trend component, there is some possibility to remain small effects due to the change of underground water level in the residuals. It has been made a rough estimation on the effects of underground water level change using the data obtained from September to November 1989 at two wells whose distances from the observation station are about 2 kilometers. At both wells, the change amounted to a few millimeters in underground water levels was observed by the atmospheric pressure change of 1 millibar. As a result, the effects of underground water level changes associated with atmospheric pressure changes will be about 10~100 times smaller than those of atmospheric pressure changes

taking the porosity of the ground into account. Therefore, even though we are ignorant about underground water level changes beneath the observation station, it will not be unreasonable to consider that the residuals will almost consist of atmospheric effects.

Atmospheric effects consist of two parts; namely, one is an atmospheric mass attraction and the other is the effect of elastic deformation caused by atmospheric mass loading. In the following of this paper, the effect of elastic deformation is called "elastic effects", which is called "elastic acceleration" in FARRELL's paper (1972). The latter is what we are interesting. By comparing the elastic effects deduced from observations with those theoretically derived from the structural earth's models, useful informations will be provided, for example, for the real response of the ocean to mass loading or for the relatively shallow structure of the earth near the observation station.

For the estimation of an atmospheric mass attraction, it is convenient to use the following expression for a distant mass from the observation station [FARRELL, (1972)],

$$g^A=-\frac{g}{4M\sin(\phi/Z)}, \qquad (1)$$

where g is the gravitational acceleration at the earth's surface and M is the earth's mass. ϕ is an angular distance between a mass and the observation station. But the thickness of atmosphere is not neglected for a near mass from the station.

Then, we directly executed the numerical integration using the assumed distribution of atmospheric mass density in the upward direction. The density of U.S. Standard Atmosphere refers to density $\rho(r)$. The attraction g^A caused by a small segment ranged by angular distance from ϕ_i to ϕ_{i+1} and direction angle from θ_j to θ_{j+1} about the

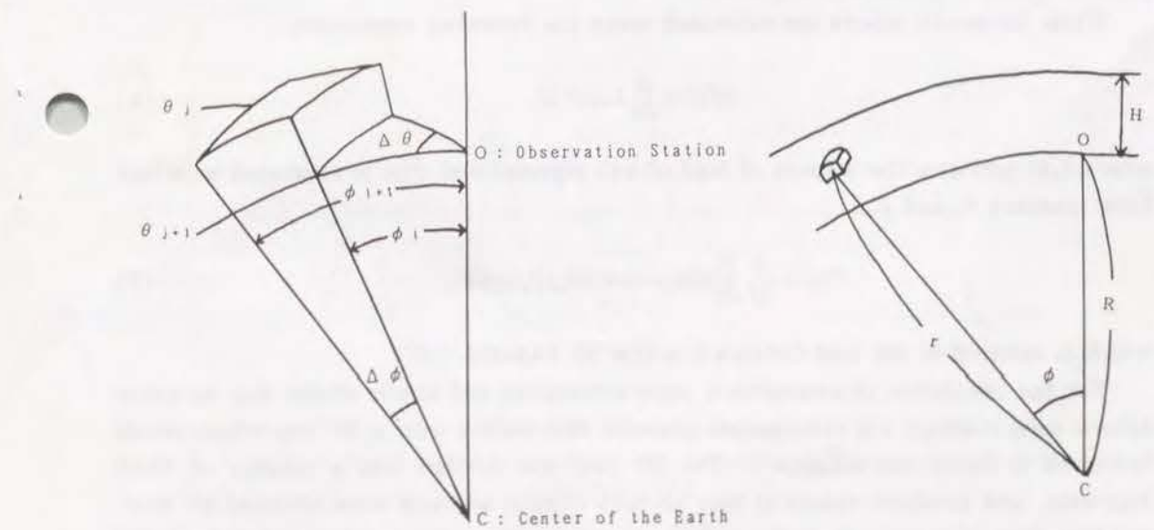

Fig. 3 Notation for calculating an atmospheric mass attraction.

observation station, as shown in Fig. 3, is expressed in the following form,

$$g^A=\int_R^{R+H}\int_{\theta_j}^{\theta_{j+1}}\int_{\phi_l}^{\phi_{l+1}}\frac{G\rho(r)r^2\sin\phi(R-r\cos\phi)d\phi d\theta dr}{(R^2+r^2-2Rr\cos\phi)^{3/2}}, \tag{2}$$

where G is the Newtonian gravitational constant and R is the earth's radius. The height of atmosphere is assumed to be 30 kilometers, where the density is only about 1.5% of that at the earth's surface. The density $\rho(r)$ is approximated as a function of the second order of distance r from the center of the earth. For the U.S. Standard Atmosphere which takes the pressure value of 1,013.25 millibars at the earth's surface, the density $\rho(r)$ is expressed by

$$\rho(r)=A(r-R)^2+B(r-R)+C, \tag{3}$$

where values A, B and C in Eq. (3) employed here are 0.0018, −0.0914 and 1.1679, respectively.

The attraction by i-th segment, whose mean atmospheric pressure is $P_i(t)$, is

$$g_i^A(t)=\alpha_i(t)\int_R^{R+H}\int_{\theta_j}^{\theta_{j+1}}\int_{\phi_l}^{\phi_{l+1}}\frac{G\rho(r)r^2\sin\phi(R-r\cos\phi)d\phi d\theta dr}{(R^2+r^2-2Rr\cos\phi)^{3/2}}, \tag{4}$$

where $\alpha_i(t)$ is defined as

$$\alpha_i(t)=P_i(t)/1{,}013.25.$$

The total attraction at time t is

$$g^A(t)=\sum_{i=1}^{N}g_i^A(t), \tag{5}$$

where N is total numbers of segments.

While the elastic effects are estimated using the following expression,

$$g^E(t)=\sum_{i=1}^{N}L_i(t)F(\phi), \tag{6}$$

where $L_i(t)$ indicates the amount of load of i-th segment and $F(\phi)$ is expressed with load Love numbers h_n and k_n,

$$F(\phi)=\frac{g}{M}\sum_{n=1}^{\infty}[2h_n-(n+1)k_n]P_n(\cos\phi), \tag{7}$$

which is referred to the load Green's function by Farrell (1972).

For the calculation of atmospheric mass attractions and elastic effects due to atmospheric mass loadings, the atmospheric pressure distribution over a 20° cap whose center is located at Kyoto was employed. The 20° cap was divided into a number of small segments, and pressure values at four corners of each segment were obtained by interpolating from the pressure values of a printed weather chart at 09 h and 21 h of JST (Japan Standard Time). The atmospheric pressure values thus employed for the

interpolation consist of several high and low atmospheric pressures, the values at 53 weather observation points in east Asia and those at 23 points which are added so as to distribute the points to be used densely near Kyoto and sparsely far from Kyoto.

Sizes of segments are distinguished into five types as follows;

$\Delta\phi=0.01°$ for $0.0°\leqq\phi<0.3°$,
$\Delta\phi=0.1°$ for $0.3°\leqq\phi<2.0°$,
$\Delta\phi=0.2°$ for $2.0°\leqq\phi<5.0°$,
$\Delta\phi=0.5°$ for $5.0°\leqq\phi<10.0°$, and
$\Delta\phi=1.0°$ for $10.0°\leqq\phi<20.0°$,

where ϕ is the angular distance from the cap's center to a mass (see Fig. 3) and $\Delta\phi$ $(=\phi_{l+1}-\phi_l)$ equals approximately to $\Delta\theta$ $(=\theta_{j+1}-\theta_j)$. Total numbers of the segments amounted to 7,790.

Figure 4 shows atmospheric mass attractions, which were thus estimated from the actual distribution of atmospheric pressures for every 12 hours; namely, 09h and 21h, in January 1-31, 1990. The residuals, in which short period tides, the linear drift and long period tides have been eliminated from original data, are also shown in Fig. 4. Figure 5 shows observed elastic effects, which are obtained by subtracting the mass attractions from the residuals, and estimated elastic effects for either case of the earth, which exists no ocean and has the ocean whose response is inverted barometer type. All values indicated in Figs. 4 and 5 are obtained as a difference from the value at January 1, 09h, 1990 (JST); namely, the first value of the analysis concerned.

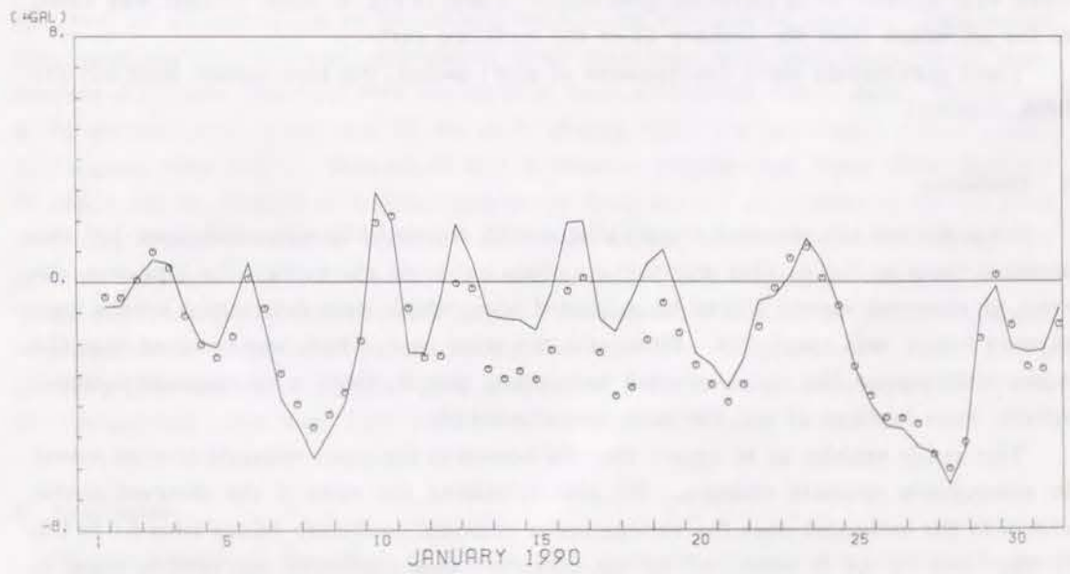

Fig. 4 Calculated atmospheric mass attractions at Kyoto (solid line).
The residuals given in Fig. 2 are also shown by circles in this figure.

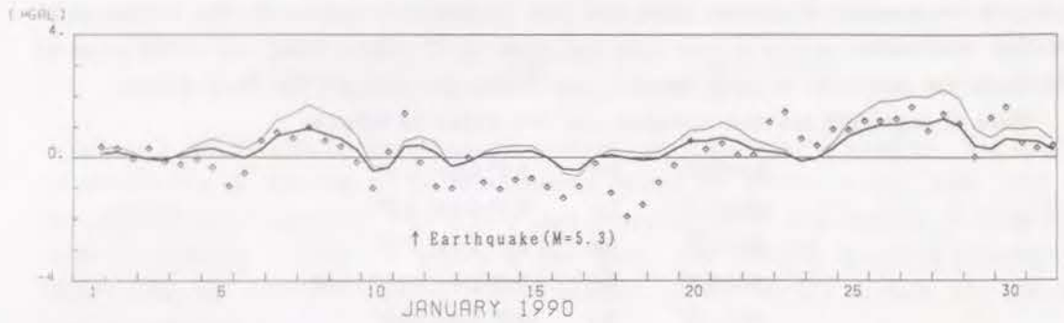

Fig. 5 Observed and estimated elastic effects.

Squares show observed elastic effects which are obtained as the difference of two kinds of values shown in Fig. 4. Thick and thin lines show estimated elastic effects whose response coefficient of the ocean is assumed to be 0.0 and 1.0, respectively. In this figure, about 0.9 μgal is added to the all values after 9h, January 12 to adjust a step caused by an earthquake occurred at 20h 11m, January 11.

After subtracting the mass attractions from residuals in which short period tides, the linear drift and long period tides were eliminated, it is considered that the remained part will consist mainly of the elastic effects due to atmospheric mass loadings. In fact, as can be seen in Fig. 5, the remained part is considerably similar to the estimated elastic effects. A large step has taken place at January 11, 20h 11m, 1990 when an earthquake occurred near Kyoto whose magnitude was 5.3. The large step was corrected in the original data, but, because of data missing for several hours after the earthquake, it remained a small step without being corrected sufficiently. Then, in Fig. 5, about 0.9 μgal was added to the all values after 9h, January 12 of the remained part.

There also remain some discrepancies of short period, but their causes have not yet been identified.

5. Discussion

We compared the observed elastic effects with theoretically estimated ones for two assumed cases in Fig. 5. One was that no ocean exists on the earth. For this case, the ratio of observed elastic effects to estimated ones, which were determined by the least squares fitting, was about 0.74. While, for the other case, which was assumed that the ocean will respond like as an inverted barometer; that is, there is no response to atmospheric mass loadings at sea, the ratio was about 1.32.

This result enables us to expect that the bottom of the ocean responds to some extent to atmospheric pressure changes. We also calculated the ratio of the observed elastic effects to the estimated ones for various ocean response coefficient values from 0.0 to 1.0. If the value of 0.4 is employed for the ocean response coefficient, the ratio is equal to almost 1.0. However, other causes must also be considered. They are, for examples, an influence of truncated errors in convolution integrals, and an influence of underground

water level changes, for which we neglected in the present study. The effect of some deviations on the earth's structure from the mean earth's model may appear as a difference in load Green's functions which can be theoretically calculated by the mean earth's structural model.

It is not so hard to be free from the influence of truncation errors by the execution of integration about the whole earth's surface employing global atmospheric pressure data, although enormous calculations will be needed. But, it is favorable to determine a range for the integration according to required accuracy. For the rough estimation of truncation errors in the present case, three assumptions were adopted; that is, the mean atmospheric pressure on the earth's surface was 1,013.25 millibars, the total load by atmospheric pressures was conserved and, at everywhere in the range out of 20° cap, pressures at a certain time were identical. In the data period concerned, a difference between maximum and minimum of the elastic effects caused by pressure changes of the outer range was about 0.02 μgal and that of mass attractions was about 0.15 μgal.

It may also be possible to obtain the ocean response and load Green's functions simultaneously by applying a linear inversion method using the data of both superconducting gravity meter and atmospheric pressure distribution. However, more data than, at least, three times or more what we used in the present study are required in order to perform this inversion. And, the influence of underground water level changes should also be estimated to perform this inversion accurately excepting the estimation of truncated errors. Changes in mass attractions due to underground water level changes affect on gravity as the same direction as those due to atmospheric pressure changes, because, when an atmospheric pressure becomes higher, an underground water level will be lower, and then, an attraction due to the underground water will also be smaller. This means that, after the corrections of atmospheric mass attractions were only made, small components of the same direction with atmospheric mass attractions will remain. Therefore, if the corrections of attractions by the underground water are performed, elastic effects may appear more clearly. Because of lack to observe underground water level, amounts of effects due to changes in underground water level can not be estimated, but we infer that they would be smaller than a half of the elastic effects induced by atmospheric pressure loadings. We are now investigating a method how to monitor the underground water level beneath the observation station. It is possible to infer the relative changes of underground water level by measuring the resistivity of ground for about a day sampling [HANADA et al. (1990)], but it needs other method to reduce to an absolute value of underground water level from the resistivity.

6. Conclusion

It was examined the effect of atmospheric pressure changes on gravity changes employing the data derived from a superconducting gravity meter and atmospheric pressure distribution within a 20° cap whose center is located at the observation station.

The elastic effects estimated from actual pressure distributions of every 12 hours were in good agreement with residuals derived by subtracting the earth tides, linear trends and atmospheric mass attractions from continuous records of gravity changes. However, there remained some discrepancies of short periods for which causes have not been identified.

The amount of observed elastic effects was generally greater than that of estimated elastic effects which were obtained under the assumption that the response is zero on the ocean. The amount was also less than that estimated under the assumption that no ocean exists on the earth. There are some possible causes to bring this result. They are non-zero response of the ocean bottom to atmospheric pressure changes, deviation in load Green's functions calculated by the mean earth's structural model, influence of underground water level changes and truncation errors of integration. Each of these problems would be interesting subject for us to be solved.

Acknowledgments

The authors wish to acknowledge Professor S. TAKEMOTO for his helpful discussions during the course of the present study. The authors wish to thank to Mr. K. FUJIMORI for his suitable suggestions on how to decrease noises caused by the room temperature variation. The authors are also indebted to the Kyoto Meteorological Observatory for offering the printed weather maps.

Numerical calculations in the present study were carried out at the Data Processing Center of Kyoto University.

References

FARRELL, W.E. (1972): Deformation of the Earth by Surface Loads, Rev. Geophys. Space Phys., **10**, 761-797.

HANADA, H., T. TSUBOKAWA and T. SUZUKI (1990): Seasonal Variations of Ground Water Level and Related Gravity Changes at Mizusawa, Tech. Rept. Mizusawa Kansoku Center, Nat. Astr. Obs., **2**, 83-93.

ISHIGURO, M., T. SATO, Y. TAMURA and M. OOE (1984): Tidal Data Analysis—An Introduction to BAYTAP—, Proc. Inst. Statis. Math., **32**, 71-85.

NAKAGAWA, I. (1962): Some Problems on Time Change of Gravity. Part 3. On Precise Observation of the Tidal Variation of Gravity at the Gravity Reference Station, Bull. Disast. Prev. Res. Inst., Kyoto Univ., **57**, 2-65.

NAKAGAWA, I., M. SATOMURA, M. OZEKI and H. TSUKAMOTO (1975): Tidal Change of Gravity by Means of an Askania Gravimeter at Kyoto, Japan, J. Geod. Soc. Japan, **21**, 6-15.

NAKAI, S. (1975): On the Characteristics of LaCoste & Romberg Gravimeter G305, Proc. Int. Lat. Obs. Mizusawa, **15**, 76-83.

OOE, M. and H. HANADA (1982): Physical Simulations of Effects of the Atmospheric Pressure and the Ground Water upon Gravitational Acceleration and Crustal Deformation, Proc. Int. Lat. Obs. Mizusawa, **21**, 6-14.

RABBEL, W. and J. ZSCHAU (1985): Static Deformations and Gravity Change at the Earth's Surface due to Atmospheric Loading, J. Geophys., **56**, 81-99.

SPRATT, R.S. (1982): Modelling the Effect of Atmospheric Pressure Variations on Gravity, Geophys. J. R. astr. Soc., **71**, 173-186.

VAN DAM, T.M. and J.M. WAHR (1987): Displacements of the Earth's Surface due to Atmospheric Loading: Effects on Gravity and Baseline Measurements, J. Geophys. Res., **92**, 1281-1286.

WARBURTON, R.J. and J.M. GOODKIND (1977): The Influence of Barometric-Pressure Variations on Gravity, Geophy, J. R. astr. Soc., **48**, 281-292.

AN ATTEMPT TO ESTIMATE LOAD GREEN'S FUNCTION FROM GRAVITY CHANGES INDUCED BY ATMOSPHERIC LOADING

Koichiro DOI

Department of Geophysics, Faculty of Science, Kyoto University

CONTENTS

Abstract

In recent years, continuous observations of gravity with time have been achieved by employing superconducting gravity meters with long-term stability and high accuracy. As a result, even small gravity changes associated with atmospheric loading are now detectable. It is, therefore, possible to obtain information about the structure of the earth from signals caused by atmospheric loading.

An attempt to estimate a load Green's function for gravity was performed using the gravity changes associated with time-varying atmospheric pressure loads. Model parameters corresponding to discrete load Green's functions were, at first, estimated by applying the conventional least squares method, but those absolute values were too large to be acceptable. A similar estimation by applying the non-negative least squares method was then performed. As a result, one parameter obtained for the nearest region was fairly well consistent with the theoretically predicted one. However, the other parameters could not be determined. The cause of such a result may be noises included in gravity changes associated with atmospheric pressure variations.

The only one parameter estimated was almost identical with the predicted one. On the other hand, absolute values of pressure coefficients of gravity observed at Kyoto were even smaller than those predicted for the earth model of a noninverted barometer type ocean. The smallness of the absolute values of pressure coefficients should correspond to a large load Green's function at the neighboring region of the observation site, and it is

considered that this discrepancy may also be due to the errors of observed data. Thus, reduction of noises such as the influence of underground water and a potent method of inversion are required for the improvement of the result.

The present method can be employed to estimate ocean response to atmospheric pressure variations. Furthermore, it is possible to apply the present attempt to a case of oceanic loading, if the change of sea level is accurately determined.

1. Introduction

Several load Green's functions for displacement, gravity, strain and tilt have been theoretically calculated for various earth structural models during the past three decades. Among them, those calculated by FARRELL(1972) based on the Gutenberg-Bullen's earth model are the most famous. Some load Green's functions for the earth model with the visco-elastic structure of the mantle were also obtained by ZSCHAU(1978) and PAGIATAKIS(1990).

The above load Green's functions have been mainly employed to correct the effects of oceanic and atmospheric loading on various geodetic and geophysical observations. After the correction of oceanic loading effects by employing convenient load Green's functions, observational results such as gravimetric tides have indicated good agreement with theoretically expected ones except for some observation sites near the coastlines(MELCHIOR et al. 1981, MELCHIOR and DE BECKER 1983). This means that the estimation of load Green's function is valuable for geodetic and geophysical studies.

On the other hand, there have been few investigations to estimate the earth's structure from observed signals induced by some loadings. ZSCHAU(1976) estimated normalized tilt Green's functions from observed oceanic tidal load tilt. He mentioned that the indirect effect of oceanic tides in tidal tilt measurements was capable of providing detailed information on the crustal and upper mantle structures by comparing the experimental normalized tilt Green's functions with theoretical ones. However,

similar investigations using the indirect effect of oceanic tides or atmospheric pressure variations in gravity have not yet been made. One of the reasons for this may be that the stability and accuracy of gravimetric observations made so far were insufficient to detect such loading effects.

According to PAGIATAKIS(1990), some influence of the visco-elastic structure of the lithosphere is dominant in the load Green's function around 0.5° of angular distance not only in its phase shift but also in amplitude change. Therefore, if the load Green's functions are accurately estimated from observations, some information about inelasticity and the deviation of structure beneath the observation site from a mean earth model can be derived. It will also be possible to make more precise corrections on the effect of oceanic and atmospheric loadings for the data obtained at each observation site.

Data obtained by superconducting gravity meters at Kyoto showed clear changes associated with atmospheric pressure variations, and atmospheric loading effects which were derived after correction for atmospheric mass attraction were in considerably good agreement with those theoretically predicted(DOI et al. 1991). It would be an advantage to employ atmospheric pressure data as the load because the data of global atmospheric pressure distribution are available at least every twelve hours and the periods of dominant pressure variations are longer than those of the principal components of the earth tides. The latter reason would simplify the procedure to detect the effect of atmospheric pressure variations from the observed data.

We thus tried to obtain the load Green's functions for gravity employing the data derived from a superconducting gravity meter (model TT-70, N009) installed at Kyoto as well as from atmospheric pressure data within 20.0° cap range whose center was located at Kyoto.

2. Data Processing

The data obtained by the superconducting gravity meter consist of tidal signals as well as non-periodic changes caused by the effects of atmospheric pressure and underground water, contribution from polar motion, instrumental drift, and others. The observed data can be expressed as follows;

$$y = \sum_j A_j \cos(\omega_j t + \phi_j) + p + D + \varepsilon \qquad (1)$$

where the first term includes the earth tides and the effect of oceanic tides, and p indicates atmospheric pressure effects in which underground water level changes caused by atmospheric pressure variation are involved. D contains the instrumental drift of the superconducting gravity meter, the effect of polar motion, crustal movements, seasonal underground water level changes and those after rainfall. ε indicates irregular noises.

In the present study, gravity changes except p and irregular noises shown in Eq. (1) should be eliminated from the hourly observed data of the superconducting gravity meter, and then, the values of 'observed elastic effects' are derived by eliminating atmospheric mass attraction from the atmospheric pressure effects p. The data period employed to get 'observed elastic effects' is about one year and four months from December 1989 to February 1991.

2.1 Eliminations of the Earth Tides, Effect of Polar Motions and Linear Trend

The tidal analysis program 'BAYTAP-G' (TAMURA et al. 1991) was applied to the data for the removal of the earth tides. After that, as can be seen in Fig. 1, an almost linear drift is superposed on the effect of atmospheric pressure. In this figure, two step-like drifts are also recognized. Their causes are still not clear, but such irregular drifts usually occurred after some shock to the gravity meter. In the succeeding data processing, irregular parts were removed and a least squares fitting was applied to the remaining data for estimating the linear drift.

Gravity changes are also induced by changes in centrifugal force caused by polar motion which consists almost entirely of the annual wobble and the Chandler wobble. Until now, the effect of polar motion has been detected in the data of superconducting gravity meters by several researchers (e.g., RICHTER 1985, DE MEYER and DUCARME 1987).

The amount of gravity changes induced by polar motion can be theoretically calculated (WAHR, 1985). According to the calculation, gravity changes amounting to nearly 10 μ gals are expected at Kyoto from the IRIS data.

Drifts in which any linear trend has been removed and the expected effects of the polar motion are shown in Figure 2. In the calculation, we assumed that gravimetric factor δ was 1.16 and phase shift was zero. In this figure, the later part of the drifts is in good agreement with the expected effects of the polar motions, but these effects were not found clearly in the

early part due to the step-like gravity changes.

Because of the shortness of the present data period and the disturbances in the early part of the drifts, the determination of amplitude and phase of the polar motion is difficult. Therefore, interpolated values of the expected effects shown in Fig. 2 were removed from the drifts in order to correct the effects of polar motion.

Fig. 3 shows atmospheric pressure variations and gravity changes associated with pressure variations during the present data period.

2.2 Estimation of Atmospheric Mass Attraction

Gravity changes associated with atmospheric pressure variations can be divided into two parts. That is,

$$p = pA + pE, \tag{2}$$

where pA is the Newtonian attraction by atmospheric mass and pE is the elastic effect induced by atmospheric pressure loadings. Atmospheric mass attraction pA can be estimated from the data of atmospheric pressure distribution around Kyoto.

Data of atmospheric pressure distributions are required to calculate the atmospheric mass attraction. In the present study, we have used printed weather charts or radio weather broadcasting to get pressure data at several tenth points in east Asia, Japan and the north-western Pacific. Many co-circle data whose center was located at Kyoto have been generated from the data of several

tenth points by interpolating. The outermost circle was placed at 20.0° angular distance from Kyoto.

The attraction of an atmospheric mass at any giventime was calculated as the summation of the attractions of small segments. One of them is shown in Fig. 4(a). The attraction of a small segment is calculated using the following expression:

$$pA = \alpha_i(t) \int_R^{R+H} \int_{\theta_j}^{\theta_{j+1}} \int_{\phi_i}^{\phi_{i+1}} \frac{G\rho(r)r^2 \sin\phi\,(R-r\cos\phi)\,d\phi\,d\theta\,dr}{(R^2 + r^2 - 2Rr\cos\phi)^{3/2}}, \qquad (3)$$

where $\alpha_i(t)$ is defined with surface pressure $p_i(t)$ as

$$\alpha_i(t) = p_i(t)/1013.25, \qquad (4)$$

and $\rho(r)$ is atmospheric mass density distribution in the direction of radius which was derived by approximating that of the U.S. Standard Atmosphere with a quadratic function as

$$\rho(r) = A(r-R)^2 + B(r-R) + C, \qquad (5)$$

where values A, B and C employed here are 0.0018, -0.0914 and 1.1679, respectively. G is the Newtonian gravitational constant and H is the height of the atmosphere. R is the radius of the earth, r is the distance between the center of the mass and the earth's center and ϕ is the angular distance between the observation site and the center of the atmospheric mass (DOI et al. 1991).

Calculations of atmospheric mass attraction were performed for 531 atmospheric pressure distribution data from December ,1989 to February, 1991. Finally, the 531 calculated attractions were removed from the corresponding gravity changes associated with atmospheric pressure variations, and the residual pEs were then obtained. Those are considered to be the values of 'observed elastic effects'.

Before estimating the load Green's function for gravity, it should be noted that the values of 'observed elastic effects' are not net values which only consist of atmospheric loading effects, but those contain unknown offsets of the superconducting gravity meter. Therefore, deviations from the initial value, namely, pE(i) - pE(1), were employed as the observed values and they are hereinafter referred to as 'observed elastic effects'. A similar procedure was also applied at the making of the loading matrix L.

The 'observed elastic effects' and predicted ones calculated with Farrell's load Green's function for gravity are shown in Fig. 5 together with atmospheric pressure variations at Kyoto during the period from December 1, 1989 to February 28, 1991.

Since we used the data of atmospheric pressure distribution within only a 20.0° range from the observation station, the effect of the outer region, namely, a truncation error, may be a cause for the error of the solution. To estimate the truncation error roughly, three assumptions were adopted. The first is that the mean atmospheric pressure on the earth's surface is 1013.25 millibars, the second is that the total load by atmospheric

pressure on the earth is conserved, and the last is that atmospheric pressure anywhere in the outer region at a given time is identical. The amount of truncation error at each time was estimated with the same method as applied for the inner region and the maximum value of mass attraction was about 0.2 μgal. While, that of elastic effects was about 0.02 μgal. These corresponding values were removed from the observed values.

3. Inverse Problem

3.1 Formation of Inverse Problem

The load Green's function for gravity is represented as

$$F(\phi) = g/M \sum_{n=1}^{\infty} [2h_n' - (n+1)k_n'] P_n(\cos\phi), \qquad (6)$$

where h_n' and k_n' are the load Love's number (FARRELL 1972). Using this Green's function, elastic effects induced by a load at a time t can be theoretically calculated, that is,

$$pE = \sum_{j=1}^{M} L(\phi_j) F(\phi_j). \qquad (7)$$

$L(\phi_j)$ is a load applied at a distance of ϕ_j from the observation station. To estimate a load Green's function from observational results, the right side of Eq. (7) is equated with the 'observed elastic effects' $pE(t_i)$, that is,

$$pE(t_i) = \sum_{j=1}^{M} L(t_i, \phi_j) F(\phi_j). \qquad (8)$$

Eq. (8) is simply expressed as follows:

$$\vec{pE} = L\vec{F}, \tag{9}$$

where $\vec{pE}$ is the vector $(pE(t_1), \ldots, pE(t_m))^T$, $\vec{F}$ is the vector $(F(\phi_1), \ldots, F(\phi_n)^T$ and L is the load matrix, whose element $L(i, j)$ at the distance ϕ_j at the time t_i is

$$L(i, j) = L(t_i, \phi_j), \tag{10}$$

and T denotes transposition.

The discrete load Green's function vector $\vec{F}$ can be obtained by solving a problem the inverse of Eq. (9), namely

$$\vec{F} = (L^T W L)^{-1} L^T W \vec{pE} \tag{11}$$

where W is the weight matrix, and the superscript -1 denotes the inverse condition.

Although we tried at present to solve only the simplest case in which the elastic earth with no ocean was assumed, it is possible to form more complicated observational equations instead of Eq. (8). When the response of the ocean to atmospheric pressure is taken into consideration, the observational equation is expressed by

$$pE(t_i) = \sum_{j=1}^{M} L^c(t_i, \phi_j) F^c(\phi_j) + L^o(t_i, \phi_j) F^o(\phi_j), \tag{12}$$

where superscripts c and o indicate the continent and ocean, respectively. Then the coefficient matrix is

$$L = \begin{bmatrix} L^c_{i1} & L^o_{i1} & L^c_{i2} & L^o_{i2} & \cdots & L^c_{in} & L^o_{in} \\ & & & \cdots\cdots & & & \\ L^c_{m1} & L^o_{m1} & L^c_{m2} & L^o_{m2} & \cdots & L^c_{mn} & L^o_{mn} \end{bmatrix}$$

and the vector $\vec{F}$ to be solved is

$$\vec{F} = (F^c(\phi_1), F^o(\phi_1), F^c(\phi_2), F^o(\phi_2), \ \cdots\ , F^c(\phi_n), F^o(\phi_n))^T$$

From the 'observed load Green's function' F, ocean response γ at the distance ϕ_j is found by

$$\gamma(\phi_j) = F^o(\phi_j)/F^c(\phi_j). \qquad (13)$$

The estimation of ocean response $\gamma(\phi_j)$ will provide significant information about interactions among the solid earth, ocean and atmosphere.

3.2 Determination of the Number of Model Parameters

Although a load Green's function in itself is a continuous function, we can only derive the function in the discrete form because of the limitation of observed data.

Since it was projected that Eq. (11) would be difficult to

solve having many parameters and an interesting feature in the load Green's function at a range less than about 2.0° for a more realistic visco-elastic earth model (PAGIATAKIS 1990), we mainly investigated the load Green's function at a range within 2.0°.

The elements $L(i, j)$ $(i=1, m,\ j=1, n)$ of the applied load matrix L consist of the loads of small segments which are distributed within the distance from ψ_j to ψ_{j+1}, ψ_j indicating one boundary of a section. $\psi_1 = 0.0°$ and $\psi_{n+1} = 2.0°$. Then the load of j-th section at the time t_i is

$$L(i, j) = \sum_{k=1}^{K_j} \sum_{l=1}^{L_k} S(k, l) P(i, k, l) / 980.25 ,$$

where $P(i, k, l)$ is the mean pressure of a segment and $S(k, l)$ is the area of the segment (see Fig. 4(b)). K_j is the number of co-circles in the j-th section and L_k is the number of segments in the k-th co-circle of the j-th section. The number n is the number of sections, and the number m equals that of observations made, that is to say the number of the 'observed elastic effects'. The boundary ψ_j was determined so as to make the area of each section almost identical.

Next, it was necessary to decide the number of model parameters to be solved within 2.0°. To determine the number of parameters, we have examined the model resolution matrix. It indicates whether the parameters can be independently predicted, or resolved. If the resolution matrix is equal to the identity matrix,

that is, diagonal elements are one and other elements are zero, then the parameters can be sufficiently resolved. If it is not the identity matrix, then the estimated parameters are weighted averages of the unknown 'true parameters'. The model resolution matrix is defined as $R = L^{-g}L$, where L^{-g} indicates the generalized inverse of L (MENKE 1989).

For various cases of the number of parameters, the model resolution matrices were investigated. As a result, the resolution matrix was far from the identity matrix when the number of parameters was greater than six. Therefore, we set the number of model parameters at five. The model resolution matrix for five parameters is shown in Table Ⅰ. Although this resolution matrix is inconsistent with the identity matrix in the strict sense, it will not induce serious problems in the results of the present study.

3.3 Solution by Least Squares Method

To solve the inverse problem according to Eq. (11), a weight matrix for observed data is required. The weight matrix W, whose elements were W(i, j) (i=1, m, j=1, m), was estimated by a Biweight-method (e.g., NAKAGAWA and OYANAGI 1982). The detailed operations to make the weight matrix are shown in Appendix A.

The results obtained for the case of five unknown parameters are shown in Table Ⅱ. The first column indicates the boundaries of a range corresponding to each parameter, and the second column is the load Green's function obtained from the 'observed elastic effects'. Predicted parameters are also shown in the third column

of this table to compare them with the observed ones. The j-th theoretical value $g_o(j)$ was calculated from Farrell's load Green's function $G(\phi)$ by the following expression,

$$g_o(j) = \left(\sum_{i=1}^{N_j} G(\phi_i)\right) / N_j \qquad (14)$$

where $N_j = (\psi_j - \psi_{j-1}) / \Delta\psi$. The last column indicates the parameters solved using theoretical elastic effects instead of the observed ones.

The parameters derived from observed data are so large when compared with the predicted ones shown in the third column that those are not acceptable. However, because the parameters obtained from theoretically calculated data in the fourth column are almost the same as the predicted ones, the discrepancies between the second and third columns might be caused by errors in the observed data.

The influence of underground water level changes after rainfall or those of seasonal changes may, especially, cause considerable observational noises. It is , however, difficult to estimate the influence without information about hydrology around observation station. Since there are no available data about underground water level, we can only estimate possible gravity changes for a simple model. We assumed a disk of aquifer with radius R placed at the depth D. Then, gravity change induced by the disk is given by

$$\Delta g = 2\pi G\rho\eta\{ d - (\sqrt{(D+d)^2+R^2} - \sqrt{D^2+R^2})\}$$

where d is thickness of the disk, ρ is density of water and η is porosity. If D=10 meters, d=1 centimeter, R=1 kilometer and η=0.1 are assumed, Δg is about 0.042 μgal. This means that twenty or thirty centimeters change in underground water level can induce about one μgal gravity change. This will become a considerable large noise.

As described above, the 'observed elastic effects' contain various noises such as the influence of underground water . To examine those or observational errors to the solution, it is convenient to use a condition indicator $\kappa(A)$ of matrix A shown in the following equation,

$$\vec{y} = A\vec{x}.$$

The definition of the condition indicator $\kappa(A)$ is given in Appendix B. As can be seen from Eq. (B-2), relative errors in the observed data vector $\vec{y}$ may appear in the solution vector $\vec{x}$ amplified by $\kappa(A)$ times. In this case, the condition indicator $\kappa(L)$ of load matrix L is about 5.0×10^{4}. This fact means that the solution of observational equation (9) is very sensitive to observational errors and not reliable (HITOTSUMATU 1982).

To examine the characteristics of $\kappa(L)$ in the present data kernel matrix L, some trial-and-error numerical experiments were carried out, and three rough tendencies were derived. The first one is that $\kappa(L)$ becomes larger according to the increment of

number of parameters to be solved. The second one is that, if the number of parameters is constant, $\kappa(L)$ takes a smaller value when the number of elements of a certain row are almost the same order. The third one is that it takes a smaller value in direct proportion to the number of observed data. The first character means that the higher is the resolution, the more unstable are the solutions. It is found from the second character that a manipulation which equalizes the area in which atmospheric loads are applied is effective to stabilize the solution. But this manipulation brings about lower resolution near the observation station and higher resolution far from it. For all these defects of the manipulation, we were able to employ it to form the matrix L.

3.4 Non-Negative Solution

As can be seen in TableⅡ, the absolute values of solutions derived by the least squares method were too large, and contained several negative values. The cause of this result is, as mentioned in preceding section, that the observational equation is sensitive to observational errors. Hence applying some constraints will make the condition of equation improve. The parameters within 2.0° should be positive, when we take the direction of gravity as positive. There was also an example of seismic inversion wherein the parameters obtained by the non-negative least squares method were considerably improved (WIDMER et al. 1991). So that, wesolved Eq. (9) again under the constraint that all of the parameters F_j (j=1, n) were non-negative, that is, minimizing $\|\vec{LF} - \vec{pE}\|$ subject to $F_j \geqq 0$.

The non-negative least squares method is a particular case of the least squares method with linear inequality constraints, namely, minimizing $\|A\vec{x} - \vec{b}\|$ subject to $C\vec{x} \geqq \vec{d}$. Since the mathematical background, details of the algorithm to solve the inverse problems under the inequality constraints and the FORTRAN program for that purpose are described in some textbooks (e.g., LAWSON and HANSON 1974, MENKE 1989), we omit them here.

Results obtained by using the non-negative least squares method are shown in Table Ⅲ, and also in Fig. 6 by dotted area. In Fig. 6, the load Green's function by FARRELL (1972) and the averaged one derived from Farrell's are also shown by solid line and shaded area, respectively. The results are much improved over those in TableⅡ which correspond to ordinary least squares

solutions. The result at the range from 0.0° to 0.89° is only slightly smaller than the predicted value, which is shown in the third column of Table Ⅲ. The other results shown in the second column of Table Ⅲ are all zero. The last column indicates the parameters derived from theoretically calculated elastic effects instead of the observed ones.

In the algorithm of the non-negative least squares method, the initial values of unknown parameters are assumed to be zero at the first stage to compute the gradient vector of total error. Here, the total error is defined as $\varepsilon(\vec{F}) = \| L\vec{F} - \vec{pE} \|^2/2$ and the gradient vector is $L(L\vec{F} - \vec{pE})$ at $\vec{F} = \hat{\vec{F}}$. And then, each of the parameters is improved from the initial value by conventional least squares methods, if the corresponding component of the negative gradient vector is positive. Therefore, if all components of the negative gradient vector become negative at the state where some of the parameters are improved from zero, the other parameters remain zero. This fact may suggest that the parameters when equal to zero can't be determined.

Since a similar analysis executed for the theoretical data set of elastic effects containing no noises showed almost equal values to the predicted parameters, the results shown in Table Ⅲ may be caused by noises included in the observed data. To examine the influence of observational errors, noises with various amplitudes determined by $\varepsilon \times (-1)^i$ were artificially applied to the theoretical data set, where ε is an amplitude of noise, and then the solutions for the data with various noises were obtained by applying the non-negative least squares method. The results of

the numerical experiments are shown in TableⅣ. This indicates that the errors of observed data must be reduced under the level of $10^{-5}\mu$gal to obtain parameters significant to two figures. It is considered that this noise level corresponds to the value of the condition indicator $\kappa(L)$.

4. Comparison between the Obtained Load Green's Function and Pressure Coefficients

As the extent of the responses of gravity to atmospheric pressure variations can be evaluated by calculating the Newtonian mass attraction and the effect of atmospheric pressure loading, a theoretical response coefficient can be obtained by adding the two effects. Thus, it is possible to justify to some extent whether the estimated load Green's function is reasonable or not by comparing the observed pressure coefficients with the theoretical response ones. Theoretical response coefficients at Mizusawa have already estimated by SATO et al. (1990) using global barometric pressure distribution. According to them, they were -0.387 and -0.296 (μgal/mb) which were calculated for the ocean of types both the inverted and the non-inverted barometer, respectively. They also mentioned that the pressure coefficient at Mizusawa by a superconducting gravity meter was -0.386 (μgal/mb).

Observed response coefficients which were obtained from the monthly data at Kyoto during the period from December 1989 to February 1991 are shown in Fig. 7 with two theoretically calculated values at Mizusawa by dashed lines. The theoretical response coefficients at Kyoto will, of course, be different from these two values at Mizusawa, but their differences must be small because the distribution of land and ocean around Kyoto doesn't differ much from that around Mizusawa. Thus, we may employ these values as criteria.

Absolute values of all the observed response coefficients are less than the theoretical value -0.387 (μgal/mb) for the ocean

of the inverted barometer type, and some of them are even smaller than that for the non-inverted barometer case(-0.296(μgal/mb)). In the effect of atmospheric pressure, the Newtonian attraction is the major component, and the elastic acceleration induced by atmospheric loading acts in the opposite direction to the Newtonian attraction. The small absolute values of response coefficients are considered to correspond to the large elastic effect. As the effect of loads at the neighborhood of the observation station is more significant, it is considered that the small pressure coefficients correspond to the large load Green's function at the neighborhood region.

The observation site at Kyoto University is not fixed on bed rock but on sediment. Large responses of the ground to atmospheric pressure loadings are therefore expected around the observation site, and the response coefficient of gravity will then take a smaller absolute value than the theoretically predicted one.

On the other hand, the result of the observed load Green's function of the nearest region in Fig. 6 or TableⅢ showed an almost identical value with the predicted one, so it appears to be incompatible with low pressure coefficients. Although its cause is not clear, as can be seen in TableⅣ, noise contamination may induce the incompatibility.

5. Concluding Remarks

An attempt to obtain the load Green's function by employing the observational data of a superconducting gravity meter at Kyoto was performed. Because of the unreliability of the coefficient matrix and contaminating observational noises, acceptable model parameters could not be estimated by the ordinary least squares method. The parameters were then estimated by applying the non-negative least squares method. One parameter derived for the nearest region from the observation station showed a relatively reasonable value while others have not yet been determined. Only one estimated parameter was almost identical with the theoretically expected value. However this fact is inconsistent with the smallness of absolute values of pressure coefficients at Kyoto.

Consequently, in order to estimate the load Green's function from observed data, it is essential to reduce observational noises. The major source of observational noise to be considered would be underground water level changes. They can be divided into two components; one is associated with atmospheric pressure variations and the other are the temporal changes after rainfall or seasonal changes. As the latter component is often fairly large, gravity changes induced by these changes seriously interfere with the determination of load Green's function. For this reason, it is very important to monitor underground water levels to obtain more reliable solutions.

In the present study, we assumed that densities at any atmospheric height were proportional to the earth's surface

pressure. The actual atmosphere, however, is more complicated than assumed. Perturbations from the atmospheric model which we employed in the present study would cause those of Newtonian attraction, and they would remain in the 'observed elastic effect' values as observational noise. If the data of atmospheric density distribution in the direction of height were available, the 'observed elastic effects' could be almost free from noise of this kind.

As shown in Table Ⅳ, it is desirable to reduce noise to the level of 10^{-5} μgal in order to accurately estimate the load Green's function. However, in practice, it is impossible to do so. Therefore, we should search for other methods to select model parameters in order to improve the condition indicator $\kappa(L)$ or more potent methods to estimate the parameters.

Although the attempt to obtain the load Green's function observationally was not successful in the present study, an investigation of this kind should be continued to clarify the heterogeneities of structures and visco-elastic characteristics within the earth. Another purpose is the correction of geodetic and geophysical data with very high accuracy.

In the present study, we employed atmospheric pressure loading as the input signal to the earth. It will be possible to make a similar attempt with load changes being effected by sea level changes, if they are accurately determined. By using two types of these loads changes, a more detailed load Green's function may be determined.

Acknowledgements

The author wishes to thank Professor Ichiro NAKAGAWA for his hearty encouragement and helpful discussions during the course of the present study. The author is also grateful to Professor Shuzo TAKEMOTO for his helpful discussions and pertinent advice. The author is indebted to Mr. Toshihiro HIGASHI for his diligent maintenance of the continuous observations by two superconducting gravity meters and the arrangement of their data. The author wishes also to thank to the National Astronomical Observatory of Mizusawa, Japan for offering the IRIS data. The author is also grateful to Professors Torao TANAKA, Norihiko SUMITOMO, Tamotsu FURUSAWA and Kazuo OIKE for their critical reading of the manuscript. The author wishes to thank Dr. Yutaka TANAKA, Dr. Kunio FUJIMORI and the members of the laboratory of Kyoto University for their valuable discussions.

Numerical calculations in the present study were carried out at the Data Processing Center of Kyoto University.

Appendix A

Diagonal components w(i) of W are calculated according to the following expression,

$$w(i) = \begin{cases} \{ 1 - (z(i)/sc)^2 \} & (|z(i)| < sc) \\ 0.0 & (|z(i)| > sc), \end{cases} \quad (A-1)$$

where z(i) is the normalized residual and it is defined as follows;

$$z(i) = v(i)/\sigma, \quad (A-2)$$

$$s = \text{median}(|z(i)|),$$

where v(i) is the deviation from the theoretical value. σ is r.m.s.e. of observed values and c is the scale factor. Components except diagonals are zero.

Appendix B

The condition indicator $\kappa(A)$ is defined as follows:

$$\kappa(A) = \|A\| \cdot \|A^{-1}\|$$

$$= \mu max / \mu min, \qquad (B-1)$$

where, $\|A\|$ means the norm of matrix A, and μmax and μmin indicate the maximum and minimum of the singular value of matrix A, respectively. Using $\kappa(A)$, the relative error of solution vector $\vec{x}$ is estimated from the following expression,

$$\|\vec{\delta}x\| / \|\vec{x}\| \leqq \kappa(A) \|\vec{\delta}y\| / \|\vec{y}\|, \qquad (B-2)$$

where $\vec{\delta}y$ is the error vector of observation vector $\vec{y}$ (NAKAGAWA and OYANAGI 1982). This expression indicates that, if $\kappa(A)$ is large, there is the possibility of a gross error through observational errors, with such cases often being called a 'sensitive problem' (e.g. HITOTSUMATU 1982).

REFERENCES

DE MEYER, F. and B. DUCARME (1987): Long Term Periodical Gravity Changes Observed with a Superconducting Gravimeter, Bull. Inform., Marees Terr., 99, 6902 - 6904.

DOI, K., T. HIGASHI and I. NAKAGAWA (1991): An Effect of Atmospheric Pressure Changes on the Time Change of Gravity Observed by a Superconducting Gravity Meter, J. Geod. Soc. Japan, 37, 1 - 12.

FARRELL, W. E. (1972): Deformation of the Earth by Surface Loads, Rev. Geophys. Space Phys., 10, 761 - 797.

HITOTSUMATU, S. (1982): Numerical Analysis, Asakura-Shoten, Tokyo, 163 p.

LAWSON, C. L., and D. J. HANSON (1974): Solving Least Squares Problems, Prentice-Hall, Englewood Cliffs, New Jersey, 340 p.

MELCHIOR, P., M. MOENS, B. DUCARME and M. VAN RUYMBEKE (1981): Tidal Loading along Profile Europe - East Africa - South Asia - Australia and Pacific Ocean, Phys. Earth Planet. Inter., 25, 71 - 106.

MELCHIOR, P. and M. DE BECKER (1983): A Discussion of World-wide Measurements of Tidal Gravity with Respect to Oceanic Interactions, Lithosphere Heterogeneities, Earth's Flattening and Inertial Forces, Phys. Earth Planet. Inter., 31, 27 - 53.

MENKE, W. (1989): Geophysical Data Analysis: Discrete Inverse Theory, International Geophysics Series, Vol. 45, Academic Press, Inc., San Diego, 289 p.

NAKAGAWA, T. and Y. OYANAGI (1982): Experimental Data Analysis by Least Squares Method, University of Tokyo Press, Tokyo, 206 p.

PAGIATAKIS, S. D. (1990): The Response of a Realistic Earth to Ocean Tide Loading, Geophys. J. Int., 103, 541 - 560.

RICHTER, B. (1985): Three Years of Registration with the Superconducting Gravimeter, Bull. Inform., Marees Terr., 94, 6344 - 6352.

SATO, T., Y. TAMURA, N. KIKUCHI and I. NAITO (1990): Atmospheric Pressure Changes and Gravity Changes, and the Applications to Geophysics, Proc. Workshop 'Searching of the Earth with Nano-Gal Level Observation', Mizusawa, 27 - 31.

TAMURA, Y., T. SATO, M. OOE and M. ISHIGURO (1991): A Procedure for Tidal Analysis with a Bayesian Information Criterion, Geophys. J. Int., 104, 507 - 516.

WAHR, J. M. (1985): Deformation Induced by Polar Motion, J. Geophys. Res., 90, 9363 - 9368.

WIDMER, R., G. MASTERS and F. GILBERT (1991): Spherically Symmetric Attenuation within the Earth from Normal Mode Data, Geophys. J. Int., 104, 541 - 553.

ZSCHAU, J. (1976): Tidal Sea Load Tilt of the Crust, and Its Application to the Study of Crustal and Upper Mantle Structure, Geophys. J. R. astr. Soc., 44, 577 - 593.

ZSCHAU, J. (1978): Tidal Friction in the Solid Earth: Loading Tides versus Body Tides, in Tidal Friction and the Earth's Rotation, eds. BROSCHE, P. and J. SUNDERMANN, Springer-Verlag, Berlin, 62 - 94.

Figure Captions

Fig. 1 Trends which were derived after the removal of the earth tides from the original data. The data period is from December 1989 to February 1991. One division of the abscissa is 10 days. Unit of figures of the ordinate is μgal. Non-linear drifts are indicated by arrows.

Fig. 2 Expected effects of polar motion on gravity and trend which was derived after the removal of the earth tides and a linear trend from the original data. The data period is the same as that in Fig. 1. One division of abscissa is 10 days and that of ordinate is 1 μgal. Effects of polar motions are indicated by circles and solid lines indicate the trend.

Fig. 3 Atmospheric pressure variation(upper) and gravity changes associated with pressure variation(lower). One division of the ordinate corresponds to 30 mb for atmospheric pressure variations and to 15 μgals for gravity changes. One division of the abscissa is one day.

Fig. 4 a) Notations to calculate atmospheric mass attraction.
An atmospheric mass is surrounded by angular distance from ϕ_i to ϕ_{i+1} and azimuth from θ_j to θ_{j+1}. H is height of atmosphere and R is radius of the earth. O is observation station.
b) Notations to calculate atmospheric pressure loading.
S(k, l) indicates the area of dotted segment and L(t, k, l) is the load imposed on the segment.

Fig. 5 Derived 'observed elastic effects' (+) and theoretical elasticeffects (○) with atmospheric pressure variation (solid line). One division of the ordinate corresponds to 30 mb for atmospheric pressure variation and to 4 μgals for gravity changes. One division of the abscissa is one day.

Fig. 6 Load Green's function for gravity estimated by non-negative least squares method. The estimated load Green's function is shown by the dotted area and the averaged one obtained from Farrell's is shown by the shaded area. A solid line indicates Farrell's load Green's function for Gutenberg's earth model.

Fig. 7 Observed response coefficients of gravity to atmospheric pressure variations obtained from monthly data to Kyoto. The data period is the same as that in Fig. 1. The upper dashed line indicates a predicted response coefficient for the earth which has the ocean of the inverted barometer type. The lower one indicates that for the earth which has the ocean of the non-inverted barometer type.

Table I Model resolution matrix for five parameters

Table Ⅱ Estimated load Green's function for gravity by the least squares method

Corresponding ranges to five parameters are shown in the first column. The estimated load Green's function from 'observed elastic effects' and the predicted one are shown in the second and third columns, respectively. In the last column, the estimated load Green's function from the theoretical elastic effects is indicated.

Table Ⅲ Estimated load Green's function for gravity by the non-negative least squares method

Corresponding ranges to the five parameters are shown in the first column. The estimated load Green's function from 'observed elastic effects' and the predicted one are shown in the second and third columns, respectively. In the last column, the estimated load Green's function from the theoretical elastic effects is indicated.

TableⅣ Influences of given noises with various amplitudes

Amplitudes of given noises are shown in the first column. Corresponding ranges to five parameters are indicated in the top row.

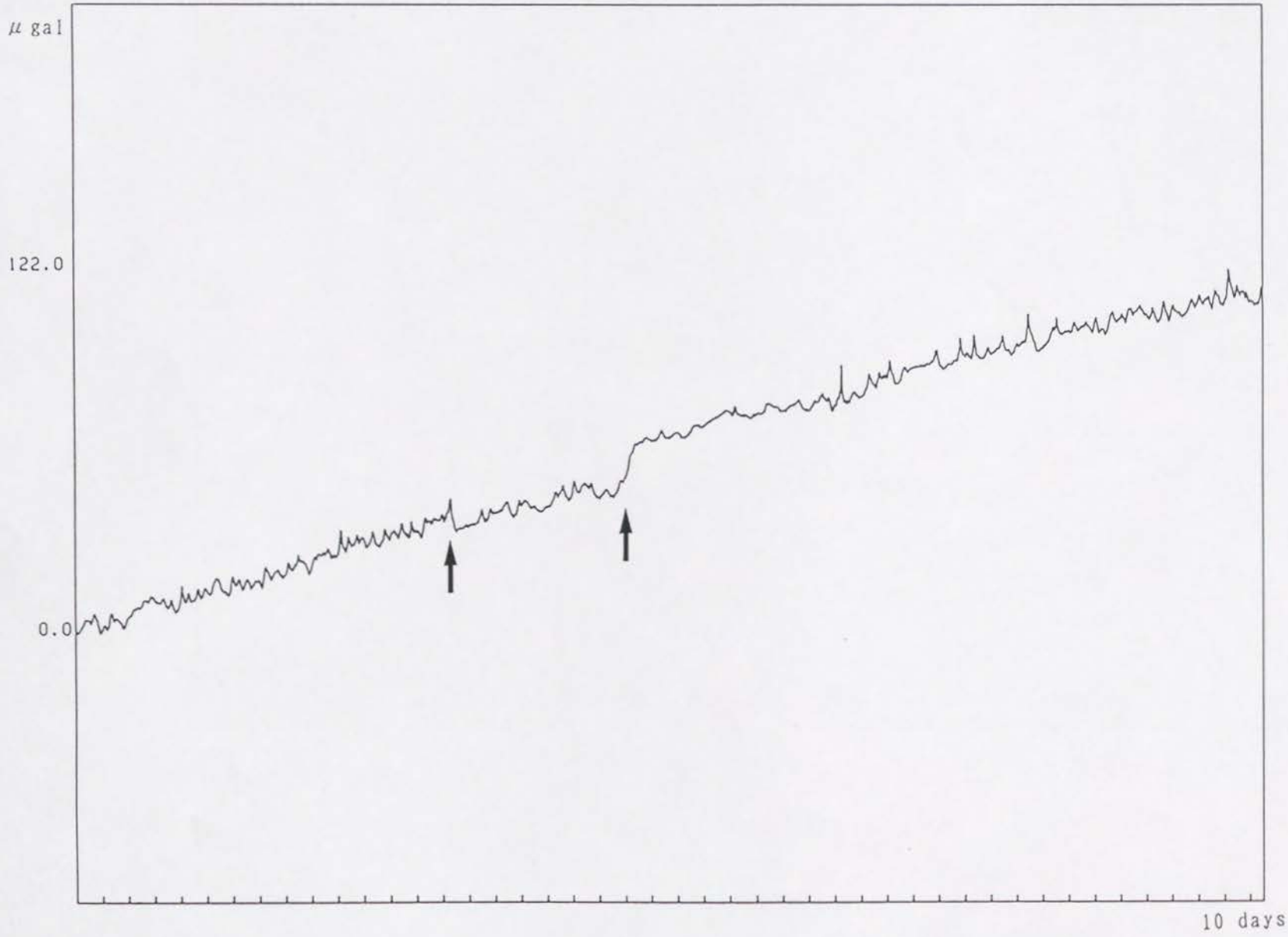

Fig. 1

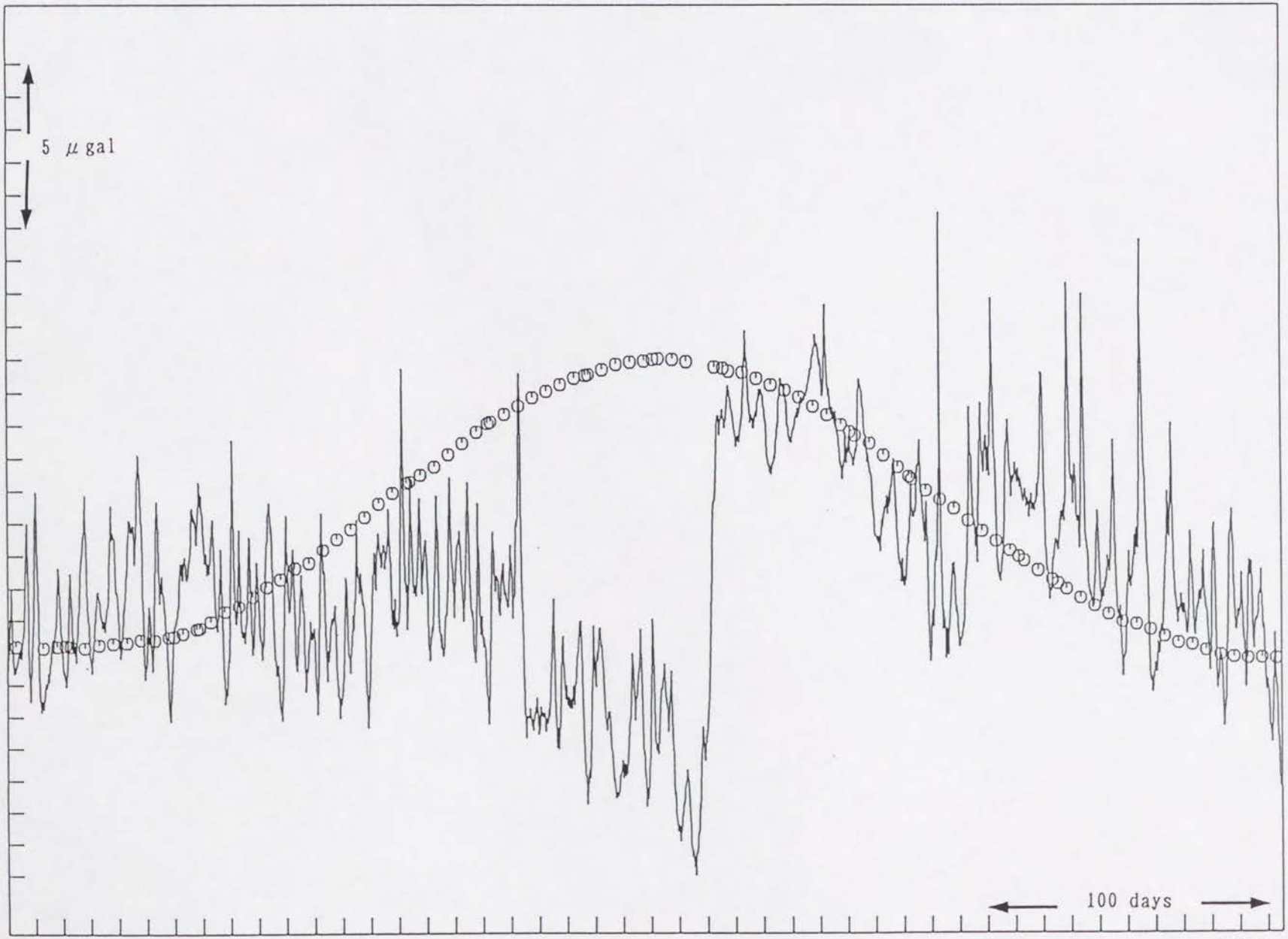

Fig. 2

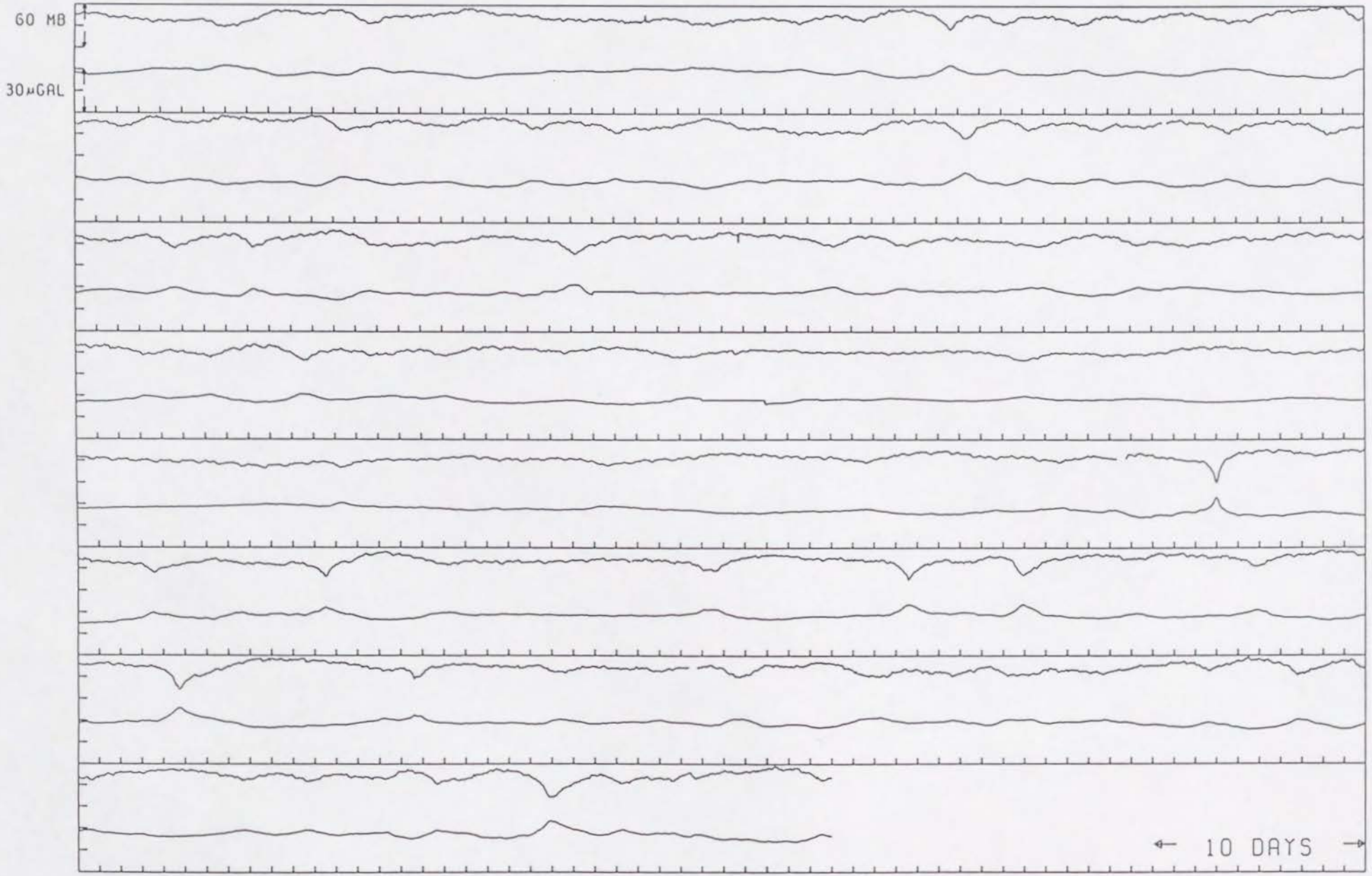

Fig. 3

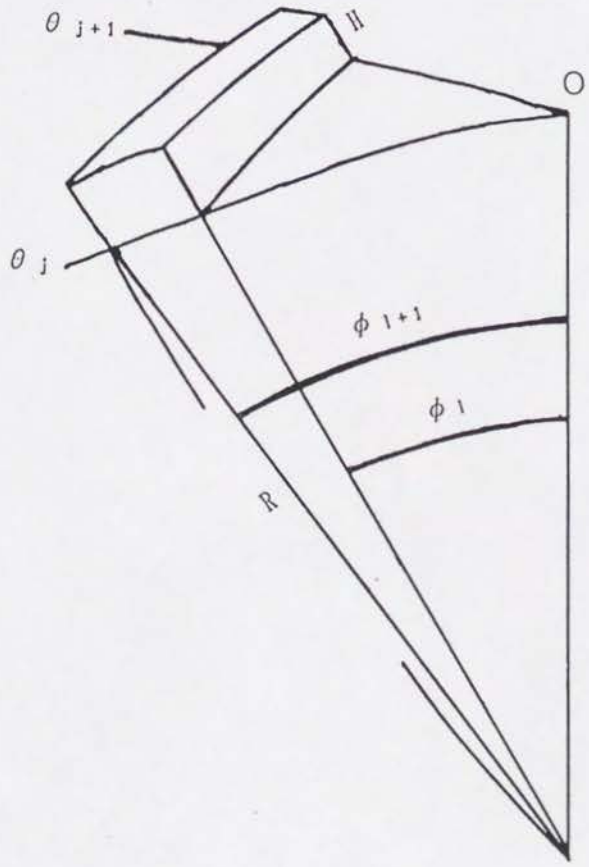

(a)

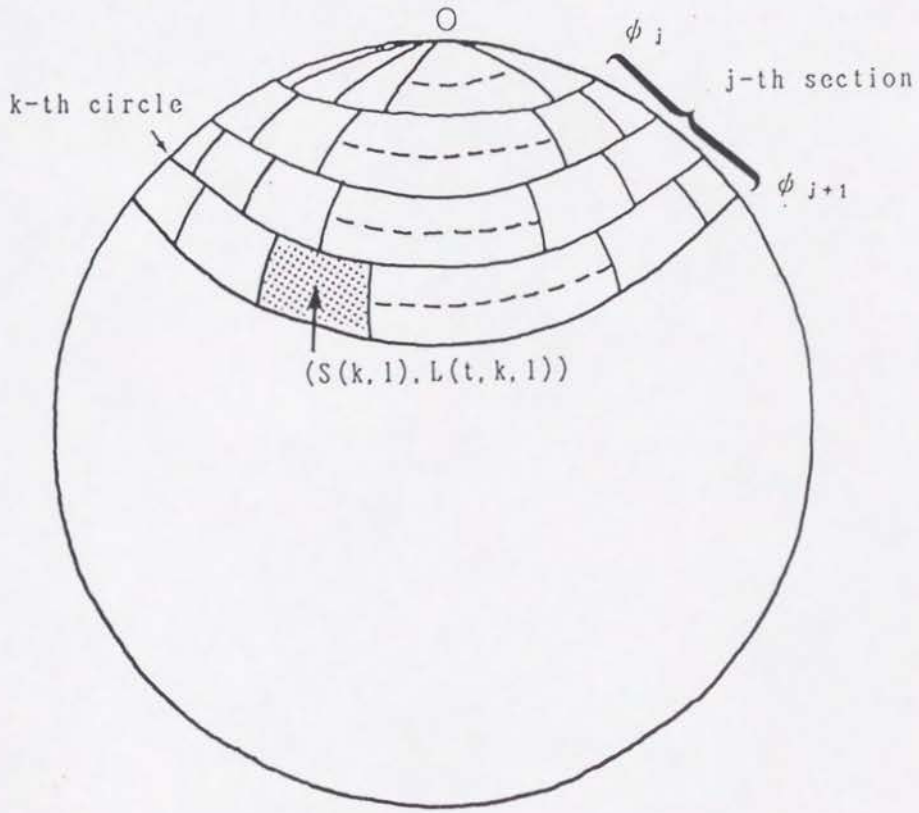

(b)

Fig. 4

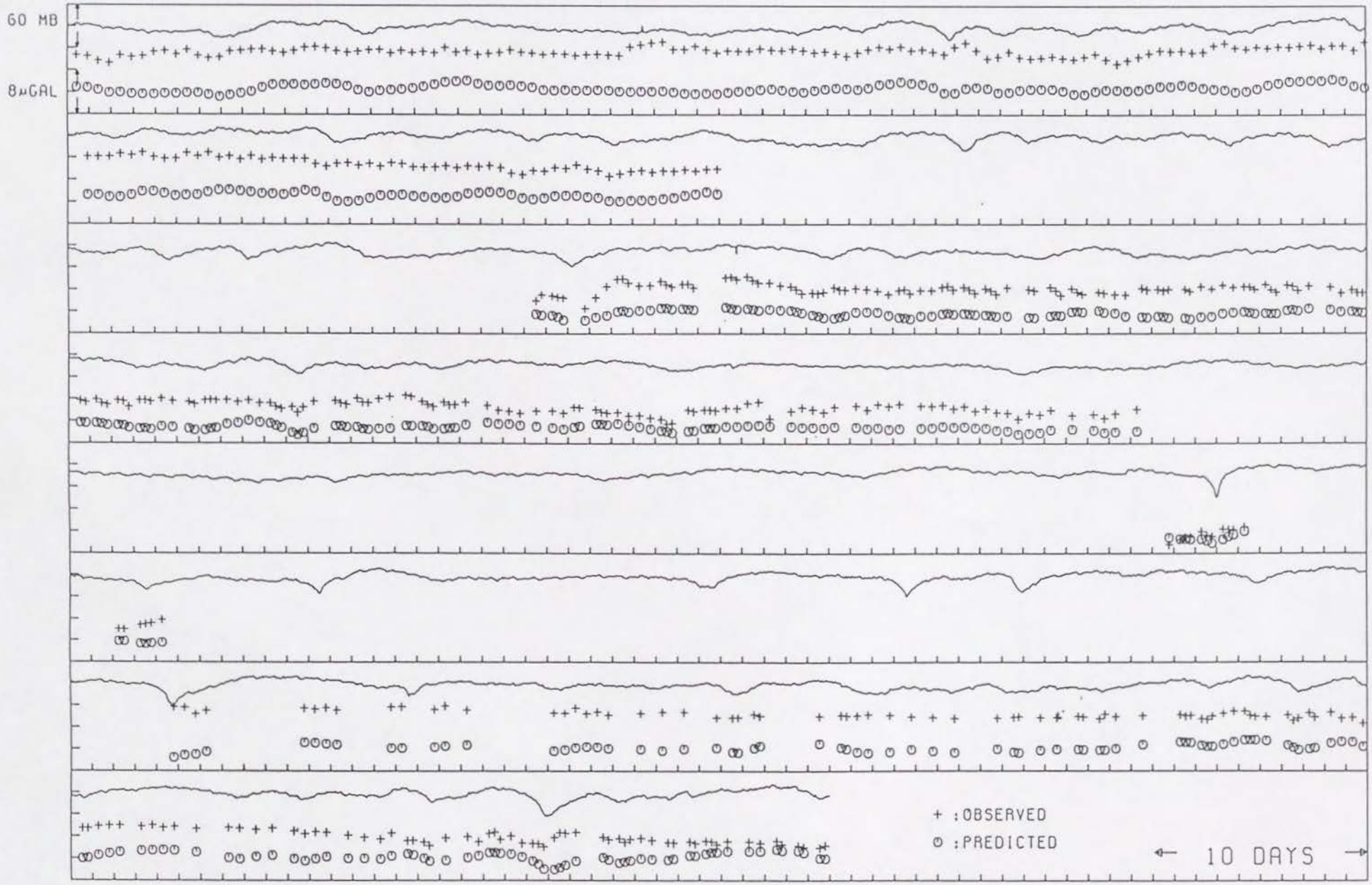

Fig. 5

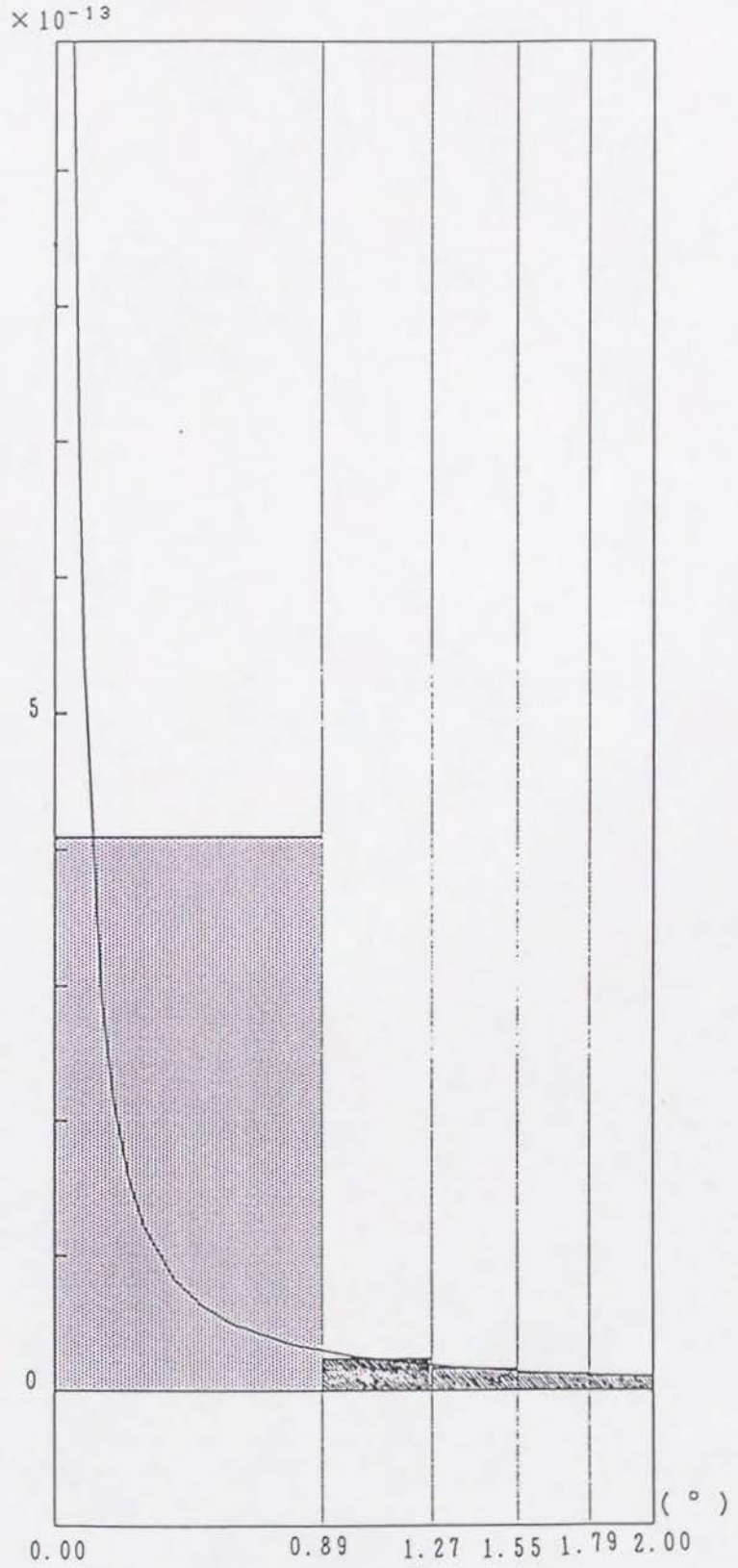

Fig. 6

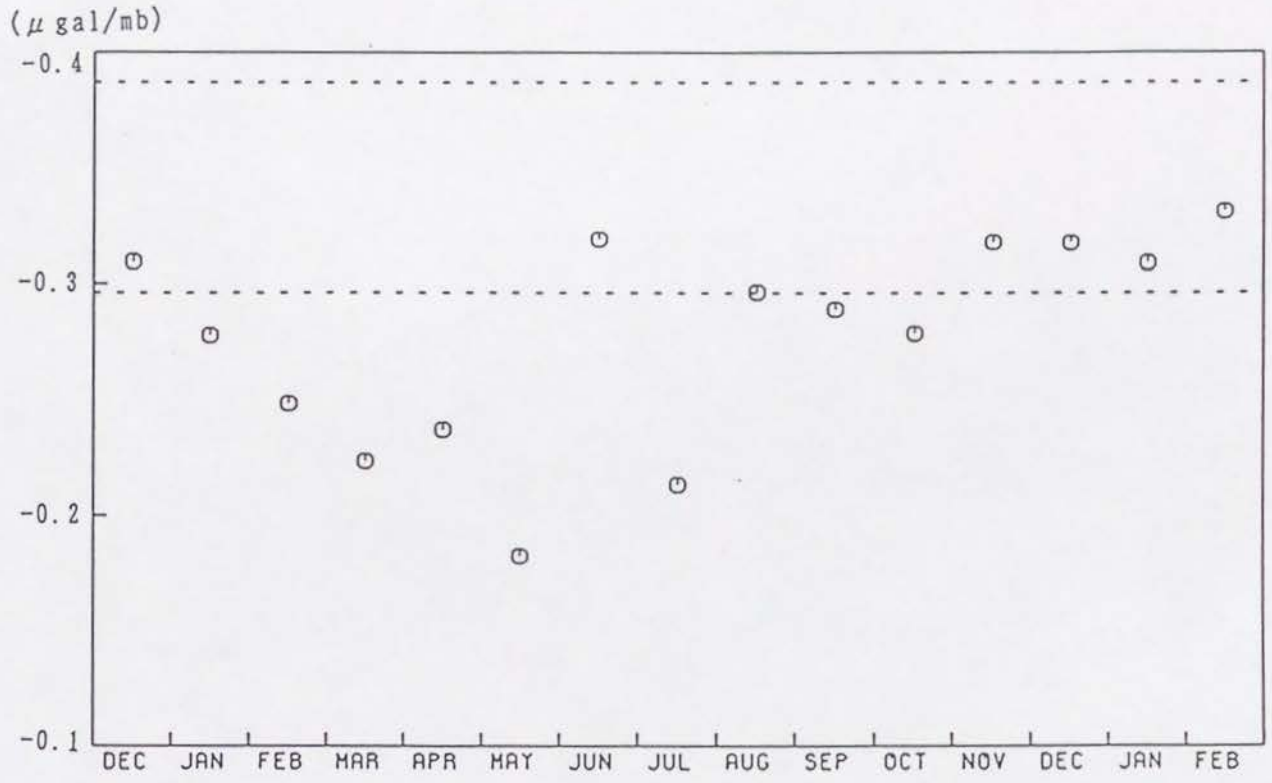
(μ gal/mb)
-0.4
-0.3
-0.2
-0.1
DEC
JAN
FEB
MAR
APR
MAY
JUN
JUL
AUG
SEP
OCT
NOV
DEC
JAN
FEB

Fig. 7

Table I

	1	2	3	4	5
1	1.009	0.011	0.007	0.012	0.009
2	0.011	1.013	0.009	0.015	0.011
3	0.007	0.009	1.006	0.010	0.007
4	0.012	0.015	0.010	1.017	0.012
5	0.009	0.011	0.007	0.012	1.009

Table II

Range (unit:degree)	Estimated Parameter	Predicted Parameter	Parameter from Theoretical Value
0.00 - 0.89	-4.05×10^{-11}	4.10×10^{-13}	4.10×10^{-13}
0.89 - 1.27	1.78×10^{-10}	2.38×10^{-14}	2.38×10^{-14}
1.27 - 1.55	-4.68×10^{-10}	1.63×10^{-14}	1.63×10^{-14}
1.55 - 1.79	1.98×10^{-10}	1.27×10^{-14}	1.27×10^{-14}
1.79 - 2.00	-7.63×10^{-11}	1.05×10^{-14}	1.05×10^{-14}

Table III

Range (unit:degree)	Estimated Parameter	Predicted Parameter	Parameter from Theoretical Value
0.00 - 0.89	4.08×10^{-13}	4.10×10^{-13}	4.10×10^{-13}
0.89 - 1.27	0.0	2.38×10^{-14}	2.38×10^{-14}
1.27 - 1.55	0.0	1.63×10^{-14}	1.64×10^{-14}
1.55 - 1.79	0.0	1.27×10^{-14}	1.27×10^{-14}
1.79 - 2.00	0.0	1.05×10^{-14}	1.05×10^{-14}

Table IV

Range (degree) / Noise (μgal)	0.00 - 0.89	0.89 - 1.27	1.27 - 1.55	1.55 - 1.79	1.79 - 2.00
1.0	2.02×10^{-13}	2.52×10^{-13}	0.0	0.0	0.0
10^{-1}	3.52×10^{-13}	1.11×10^{-13}	0.0	0.0	0.0
10^{-2}	4.11×10^{-13}	0.0	7.76×10^{-14}	6.37×10^{-15}	0.0
10^{-3}	4.13×10^{-13}	7.78×10^{-15}	5.46×10^{-14}	1.89×10^{-16}	1.33×10^{-14}
10^{-4}	4.10×10^{-13}	2.22×10^{-14}	2.01×10^{-14}	1.14×10^{-14}	1.07×10^{-14}
10^{-5}	4.10×10^{-13}	2.37×10^{-14}	1.67×10^{-14}	1.26×10^{-14}	1.05×10^{-14}
0.0	4.10×10^{-13}	2.38×10^{-14}	1.63×10^{-14}	1.27×10^{-14}	1.05×10^{-14}